Proceeding of the 14th International Forum of Automotive Traffic Safety, 2017, pp 344-358
No.ATS.2017.412

Theoretical design and numerical study of thin-walled structures formed with L- and T- shape elements for crashworthiness under axial loading

Chao Gonga, Zhonghao Baia*, Binhui Jianga,b

a State Key Laboratory of Advanced Design and Manufacturing for Vehicle Body, Hunan University, Changsha, Hunan 410082, PR China

b Bioengineering Center, Wayne State University, MI 48201, USA

**Corresponding Author: E-mail: baizhonghao@hnu.edu.cn*

Abstract: Multi-cell thin-walled tubes have attracted a considerable amount of attention for their excellent energy absorption capacity. In this paper, a folding and translation method based on SSFE theory was proposed to design the cross-sectional of multi-cell thin-walled tubes. Based on this method, three types of multi-cell thin-walled tubes with different cross-sectional configurations were generated to compare the energy absorption capacity by theory analysis and numerical simulation. It is found that the crashworthiness of the Tube Type Ⅲ, which was changed from the Tube Type Ⅰ by using folding and translation method, is better than that of the other two multi-cell thin-walled tubes under axial impact. Then, a parameter study was carried out for the Tube Type Ⅲ to investigate the influence of cross-sectional geometric parameters in energy absorption capacity. It is concluded that the wall thickness, the corner-cell size and flange locations have obvious effect on the crashworthiness of the multi-cell thin-walled tubes.

Keywords: Multi-cell thin-walled tubes, Folding and translation method, Crashworthiness, Axial impact

1 Introduction

Due to the excellent energy absorption capacity, thin-walled structures have been widely applied as energy absorbers in aerospace, automotive, military equipment and other industries for their excellent energy absorption capacity and lightweight [1-4]. For an energy absorption device, crashworthiness is an important ability to protect the vehicle itself and its occupants from serious injury or death when it is subjected to an impact load [6]. In order to improve the energy absorption capacity of the thin-walled structure, many researchers have made their contribution to investigating different design methods and exploring energy absorption laws for various conditions from quantities of experiments [7-12], numerical simulations [13-18] and theoretical analysis [19-23].

In the 1960s, Alexander [24] was the first to focus on being able to obtain an approximate theoretical expression of the mean axial crushing force for thin-walled circular tubes. In 1983, the Super Folding Element (SFE) theory was proposed by Wierzbicki and Abramowicz [25] to investigate theoretical mean crushing force prediction of rectangular tubes under axial impact. Chen and Wierzbicki [26] investigated the energy absorption of the square tubes with single-cell double-cell and triple-cell under axial loading. To simplify the SFE theory, the kinematical admissible of SFE [25] was replaced with a basic folding element to model both the bending action, modeled using three stationary hinge lines over each flange, and membrane action, characterized by three extensional triangular elements near the corner line. They obtained an analytical mean crush force equation by dividing the tube cross-section into distinct panel section and angle element, and establishing contact between the fractional energy absorption of each flange and its parameters of thickness and length. In addition, Kim [5] employed Chen and Wierzbicki's model to investigate the multi-cell square tubes with four square cells locating at the corners. It was concluded that the SEA of new multi-cell square tubes increased by 1.9 times, compared with conventional square tube.

Zhang et al. [27] investigated square columns with $n \times n$ square cells in the cross-section and three type of basic folding elements (L-shape, T-shape and crisscross shape). It is found that the energy absorption efficiency of a single-cell column can be increased by 50% when the section is divided into 3×3 cells. Zhang and Cheng [28] put forward that the multi-cell square columns with different configurational sizes could absorb about two times more energy than the foam-filled square columns with the same weight. Zhang and Zhang [29] carried out the quasi-static axial compression experiments for multi-cell square tubes with different sections. The result indicated that multi-cell square tubes are much more efficient than hollow tubes in energy absorption under axial impact. Wu et al. [30] compared the crashworthiness of three tubes with one, four and five cells. It is found that both MCF and SEA of multi-cell tubes increase with the number of cells. Furthermore, they investigated energy absorption efficiency of five-cell tubes through parameter study and multi-objective optimization and obtained an optional five-cell tube.

According to the theoretical studies, it can be found that the number of basic elements can be significantly effect on the crashworthiness of thin-walled structures [25,43]. However, no theoretical design method was developed for the crashworthiness of thin-walled structures based on this detection. In this study, a new crashworthiness design method named folding and translating wall method was proposed to improving the energy absorption capacity by increasing the number of structure's basic elements and implemented on an initial structure (Tube Type I [5,30]) formed with L and T shape elements. After folding and translating the wall of initial structure, two new structures (Tube Type II and Tube Type III) with more basic elements were obtained. For these three structures, all geometric parameters are the same expect for geometry cross-section configuration. Then, numerical simulations were conducted to investigate and compare the actual energy absorption capacity of these three structures. The results of numerical simulations predicted that the Tube Type III structure with most basic elements showed the best energy absorption capacity. Finally, a parametric study was carried on the Tube Type III structure to advanced investigate the influences of the wall thickness, the location of the connecting flange walls and the size of the corner-cell on the energy absorption capacity.

2 Theoretical analysis

2.1 The simplified super folding element theory

In 2001, Chen and Wierzbicki [26] proposed that the external work applied by compression was dissipated by plastic deformation in bending and membrane. This proposes can be expressed as [27-29]:

$$2HP_m k = W_{bending} + W_{membrane} \tag{1}$$

where H and P_m denote the half-length of a folding and the mean crushing force over the collapse of a folding, respectively, $W_{bending}$ and $W_{membrane}$ are the energy dissipation in bending and membrane deformation, respectively. Considering the actual folding element can never be completely flattened, an effective collapse coefficient k was used in this equation. Usually, the effective collapse coefficient k lies in the range of 70-75% [25].

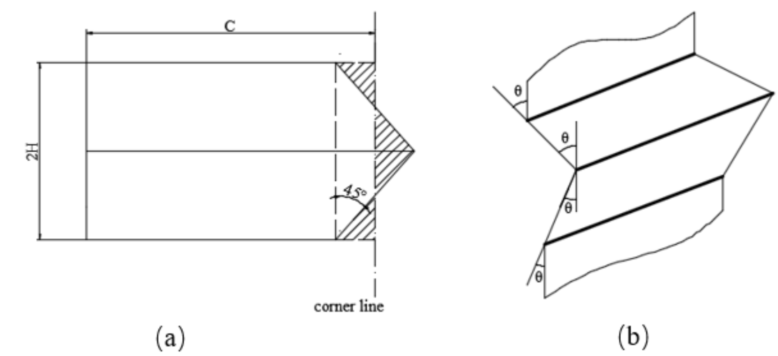

Fig.1 Scheme of the simplified super folding element (SSFE) [26]: (a) extensional elements, (b) bending hinge lines

The bending energy $W_{bending}$ can be calculated by summing up the energy dissipation at stationary hinge lines. For each flange, three horizontal stationary hinge lines are developed (Fig. 1(a)). Therefore, the bending energy could be expressed as follow:

$$W_{bending} = \sum_{i=1}^{3} M_0 \varphi_i L_c \tag{2}$$

where $M_0 = \sigma_0 t^2/4$ denotes the fully plastic bending moment of the flange and t is the wall thickness of the multi-cell thin-walled tube. σ_0 is the flow stress of material with power law hardening; φ_i is the rotation angle at each hinge line and L_c denotes the total length of all flanges. For simplicity, it is assumed that the flanges are completely flattened (Fig.1(b)) after the axial compression of 2H [26], which means that the rotation angles at the three hinge lines are $\pi/2$, π and $\pi/2$, respectively (Fig.2). Consequently

$$W_{bending} = 2\pi M_0 L_c = \frac{\pi\sigma_0 t^2 L_c}{2} \tag{3}$$

where L_c is the total length of the wall the cross-section. σ_0 is flow stress of structural material. And it could be calculated by [20,37]

$$\sigma_0 = \sqrt{\frac{\sigma_u \sigma_y}{1+n}} \tag{4}$$

where σ_u and σ_y denote the ultimate stress and the initial yield stress, respectively. n is power law exponent of the structural material.

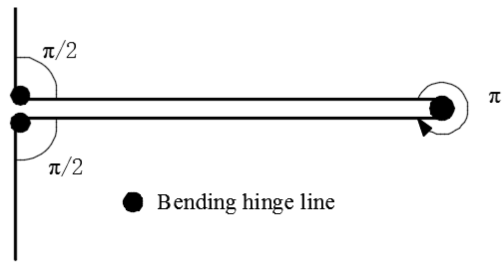

Fig.2 Bending hinge line and rotation angle on basic folding

The membrane energy $W_{membrane}$ dissipated during one wavelength crushing can be calculated by integrating the extensional and compressional areas. The membrane energy of the corner element and $T-$shape element are discussed in the following [23]:

$$M_{L-shape} = \frac{4M_0H^2}{t} \tag{5}$$

$$M_{T-shape} = \frac{12M_0H^2}{t} \tag{6}$$

Therefore, the whole membrane energy can be calculated by

$$W_{membrane} = N_L M_{L-shape} + N_T M_{T-shape} \tag{7}$$

where N_c and N_T denote the number of corner and T-shape, respectively.

Substituting the terms of Eq. (3), (7) into Eq. (1), the general theoretical equation of the mean crushing force of multi-cell thin-walled tube was obtained. It is

$$\begin{aligned} 2HP_m k &= 2\pi M_0 L_c + N_L M_{L-shape} + N_T M_{T-shape} \\ &= 2\pi M_0 L_c + 4(N_L + 2N_T)M_0 H^2/t \end{aligned} \tag{8}$$

Transforming Eq. (8), it is

$$\frac{P_m k}{M_0} = \frac{\pi L_c}{H} + \frac{2(N_L + 2N_T)H}{t} \tag{9}$$

The half-wavelength H can be obtained under the stationary condition of the mean crushing force:

$$\frac{\partial P_m}{\partial H} = 0 \tag{10}$$

Then

$$H=\sqrt{\frac{\pi L_c t}{2(N_L+2N_T)}} \tag{11}$$

Substituting Eq. (11) into Eq. (9), the mean crushing force for a multi-cell section under quasi-static impact could be obtained:

$$P_m=\frac{2M_0\sqrt{2(N_L+2N_T)\pi L_c/t}}{k}=\frac{\sigma_0 t\sqrt{2(N_L+2N_T)\pi L_c t}}{2k} \tag{12}$$

However, this expression is unsuitable for dynamic case since it did not take the effects of dynamic loading into account. In dynamic loading case, the dynamic amplification effects, including inertia and strain rate effects should be considered. In fact, the aluminum alloy with No. AA6 series is insensitive to the strain rate [36], so strain rate effect could be neglected. In order to consider the inertia effect, a dynamic enhancing coefficient λ was brought in. According to the previous investigations [37-39], the value of the coefficient λ is in the range of 1.1-1.6 for aluminum. Therefore, the theoretical equation of the mean crushing force of multi-cell thin-walled tube under dynamic loading is descripted as:

$$P_m^{dym.}=\lambda\frac{\sigma_0 t\sqrt{2(N_L+2N_T)\pi L_c t}}{2k} \tag{13}$$

2.2 The folding and translating wall design method

From the Eq. (1), it can be observed that increasing total dissipative energy of the structures can be achieved by increasing the bending energy and membrane energy. In order to increase the bending energy, one or more of the material flow stress σ_0, thickness t and the total length of the wall the cross-section L_c should be increased. However, the mass and peak impact force of the structures also would be increased with increasing the thickness t and the total length of the wall the cross-section L_c [23,39, 45]. If the structures with high mass and peak impact force will be used as energy absorption devices for the vehicle safety, they are not conducive to lightweight and occupant protection [30,46]. Therefore, most of researchers considered to increase the material flow stress. For example, more and more new materials with high flow stress were used to develop the energy absorbing devices [30,47]. For the membrane energy, it can be seen that it is determined by the corner numbers and the basic element types. In some studies, new cross-sectional configurations were designed by increasing the total length and number of basic elements to improve the energy absorption capacity of structures [27-29]. Considering the lightweight, the final mass of structure also was an important factor in these studies [6,44]. Therefore, the folding and translating wall design method for the development of energy absorption structure was proposed that only the number of basic elements was increased to obtain the new cross-sectional configuration. The detailed processing of this new method was described as follows. Fig.3 shows the cross-sectional configurations of multi-cell thin-walled tubes by folding and translation method. Tube type Ⅰ has been proved that it is a good energy absorber in the previous investigation. [30]. To demonstrate the variation from Tube type Ⅰ to Tube type Ⅱ, the folding method is applied to fold four right corner of Tube type Ⅰ. Then, Tube type Ⅲ could be obtained from Tube type Ⅱ by translating the flanges, which is connected the four corner cells. In these three new structures, Tube type Ⅱ has eight more right corner elements compared with Tube type Ⅰ. Tube type Ⅲ has eight more right corner elements than Tube type Ⅱ.

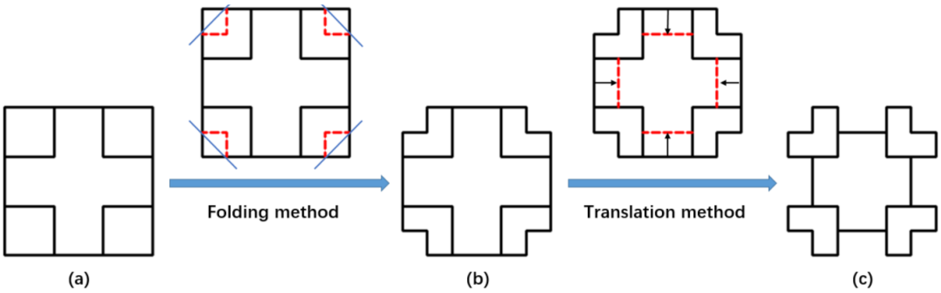

Fig.3 Cross-sectional configurations of multi-cell thin-walled tubes by folding and translation method

In order to compare the actual energy absorption capacity of these three structures, the theoretical absorptive energy was calculated according to eq. (13). In the calculation processing, the material flow stress σ_0, effective collapse coefficient k, wall thickness t, and total wall length L_c of these three structures were assumed and defined as 175.86 MPa, 75%, 1.6 mm, and 510 mm, respectively. The dynamic enhancing coefficient λ for these three structures were set as 1.1, 1.15 and 1.2, respectively. The other data for the analytical evaluation are listed in Table 1. The final theoretical values of three structures' mean crushing force were compared and shown in Table 2. It can be found that, the value of mean crushing force for Tube Type Ⅱ was increased by 16.89% than that of Tube Type Ⅰ, while the value of mean crushing force for Tube Type Ⅲ was 1.34 times than that of Tube Type Ⅰ. Obviously, the value of mean crushing force was increased with increasing of the corner numbers.

Table 1 Input data for the theoretical evaluation of the mean crushing force

Structure	Tube Type Ⅰ	Tube Type Ⅱ	Tube Type Ⅲ
Number of L-shape	8	16	24
Number of T-shape	8	8	8
P_m^{dym}(kN)	90.631	105.935	121.091

3 Finite element modeling

3.1. crashworthiness indicators

To quantitatively evaluate the crush characteristics and energy absorption of different structures, there have been a number of the crashworthiness indicators. The specific energy absorption (SEA) indicates the absorbed energy per unit mass of the crashed structure as:

$$\mathrm{SEA} = \frac{\mathrm{EA(d)}}{\mathrm{m}} \tag{14}$$

where d denotes the axial crushing distance, which is taken as 120 mm in this study. m is the total mass of the multi-cell tubes and EA is the total energy absorbed during crushing process, calculated as:

$$\mathrm{EA} = \int_0^{\mathrm{d}} \mathrm{F(x)dx} \tag{15}$$

where $\mathrm{F(x)}$ is the instantaneous crashing force with a function of the deformation x.

IPF is defined as the initial peak force in the compaction zone. The excessively high IPF is undesirable since it will result in a large deceleration, therefore, IPF should be decreased for the safety of occupants and to minimize the structural damage [40-42]. MCF for a given deformation d can be calculated as:

$$MCF = \frac{EA(d)}{d} \tag{16}$$

3.2. FE model

Although the theoretical solutions of these three structures' absorption energy were calculated and compared, the Finite element method was still used to advanced study the crashworthiness of them. Based on the explicit nonlinear FE code LS-DYNA (Version 971, LSTC, Livermore, CA, USA), the FE models which were simulated the axial impact were established and showed in Fig.4. the length L of thin-wall structures, the width b and the size of corner cell C was 200 mm, 90 mm, and 30mm, respectively.

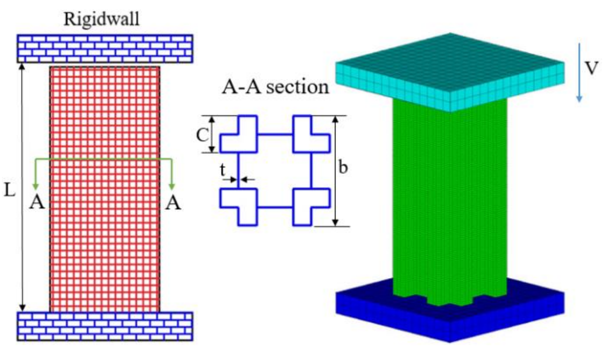

Fig.4 Finite element modeling of multi-cell thin-walled tube

In the models, the multi-cell thin-wall structure was placed in the middle of two rigid plates. One of the rigid plate is used to fixed the tube, and another one is a rigid wall. The rigid wall is moved downwards from the top of tubes with a prescribed velocity boundary condition to compress the multi-cell tubes in the axial direction. The load velocity is kept constant as 10m/s. The multi-cell tube is modeled using four-load shell elements with five integration points in the element plane, which was formulated by Belytschko and Tsay. Stiffness-based hour-glass control is employed to avoid spurious zero energy deformation modes. The element size of the multi-cell tube is 2mm. The structure material AA6063 T5 is modeled with material model MAT 123 (modified piece-wise linear plasticity material model) in LS-DYNA. Two types of contacts are employed in the numerical analysis. The first is to model the interface between the rigid plates and wall of column by using the automatic surface to surface contact algorithm. The second is to avoid interpenetration of tube folding during axial collapse by using the automatic single surface contact algorithm. The static and dynamic frictional coefficients defined are taken as 0.2 and 0.3 in these contacts, respectively.

The material of the multi-cell thin-walled structure here is aluminum alloy AA6063 T5 with mechanical properties: Young's modulus $\mathrm{E} = 68.2\mathrm{GPa}$, Poisson's ratio $\mu = 0.3$, density $\rho = 2.7 \times 10^3 \mathrm{kg/m^3}$, initial yield stress $\sigma_{y0} = 180\mathrm{MPa}$, the ultimate tensile stress $\sigma_u = 206\mathrm{MPa}$ and the power law exponent n is 0.199. The engineering stress-strain curve of this material is shown in Fig.5.

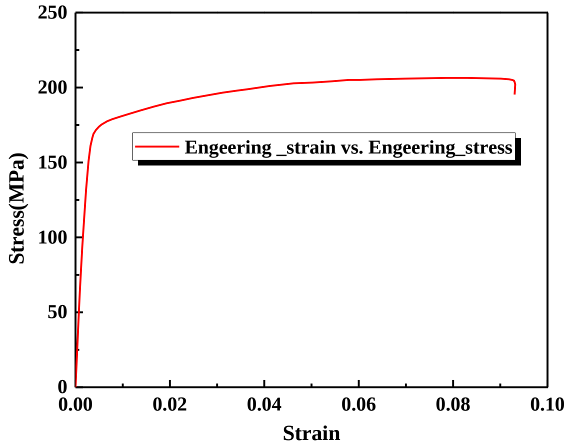

Fig.5 The stress-strain curves of Al6063-T5 [30]

3.3. Comparisons the results predicted by FE models and theoretical formula

The numerical results of these multi-cell tubes under axial impact could be compared with the theoretical formula results to validated the FE models. For every type of tubes, six different thickness values (1mm, 1.2mm, 1.4mm, 1.6mm, 1.8mm and 2.0mm) are chosen to validate the accuracy of the FE models.

Table2 The errors among FE numerical results and theoretical predictions for the three structures

	Tube Type Ⅰ			Tube Type Ⅱ			Tube Type Ⅲ		
t(mm)	MCF(kN)	P_m(kN)	Error(%)	MCF(kN)	P_m(kN)	Error(%)	MCF(kN)	P_m(kN)	Error(%)
1.0	43.258	44.782	3.522	50.401	52.343	3.853	58.034	59.832	3.099
1.2	58.028	58.867	1.447	66.939	68.807	2.791	80.335	78.651	-2.096
1.4	71.702	74.181	3.457	85.328	86.706	1.616	99.479	99.112	-0.369
1.6	90.802	90.631	-0.187	105.274	105.935	0.628	120.210	121.091	0.733
1.8	109.818	108.145	-1.523	129.524	126.406	-2.407	152.734	144.491	-5.397
2.0	134.539	126.611	-5.855	153.418	148.049	-3.500	160.130	169.230	5.683

The relative errors among FE numerical results and theoretical predictions for these three structures is shown in Table 2. According to the data of Table2, it can be seen that the results predicted by FE models and theoretical formula are almost fitness and the maximum error is less than 6%. Therefore, it can be concluded that the theoretical formula and FE models established in this paper is sufficiently accurate.

3.4 Crashworthiness of the three thin-walled structures

Fig.6 showed crashworthiness performance comparisons for three structures with different wall thickness. According to Fig.6 (a), it can be seen that values of IPF increased with the increasing values of wall thickness and the values of IPF were close for three structures with same thickness. Fig.6 (b), (c) and (d) showed that the values of MCF, SEA and CLE for three structures increased with the increasing values of wall thickness. For a certain wall thickness value, the values of MCF, SEA and CLE for the Tube Type Ⅲ is larger than that of the other two structures.

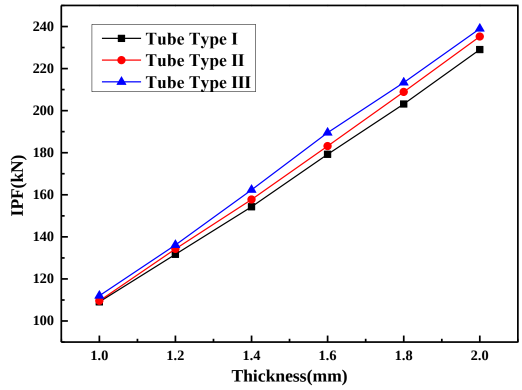

(a)

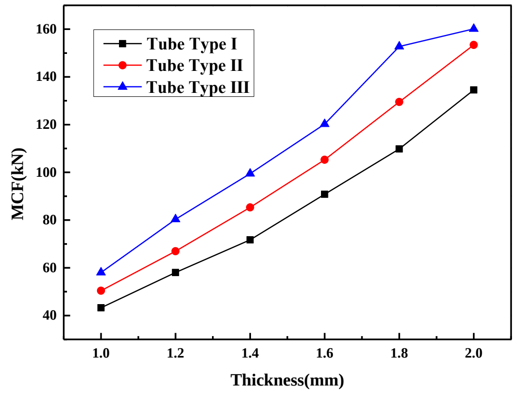

(b)

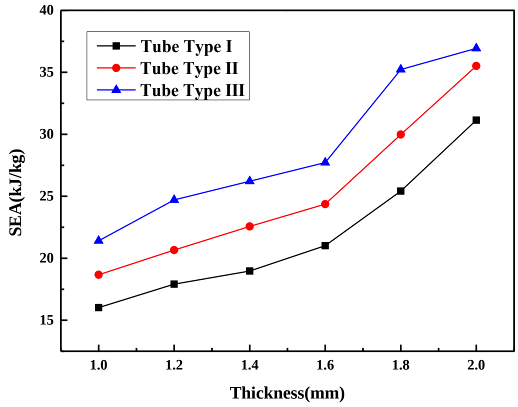

(c)

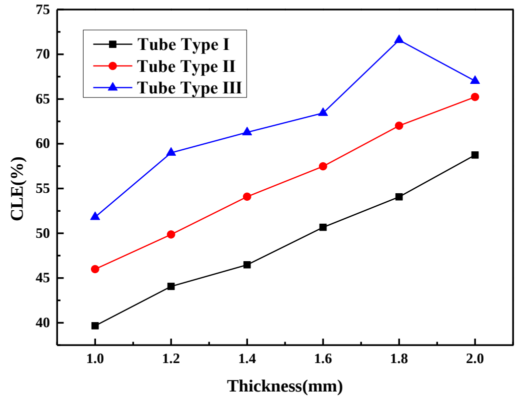

(d)

Fig.6 Performance comparisons for three structures: (a) IPF, (b) MCF, (c) SEA, and (d) CLE

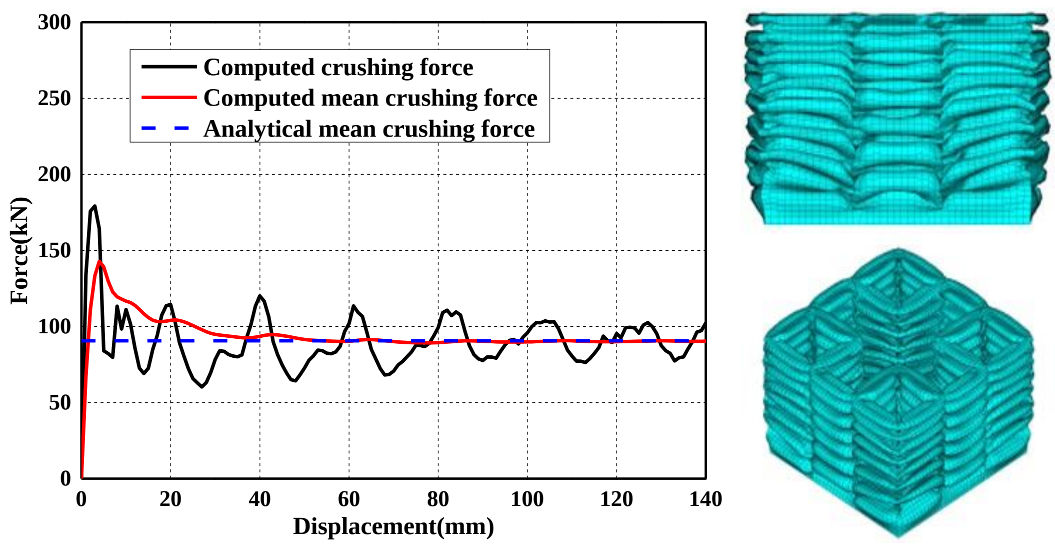

Fig.7 Crushing force and deformed structure with Tube Type Ⅰ

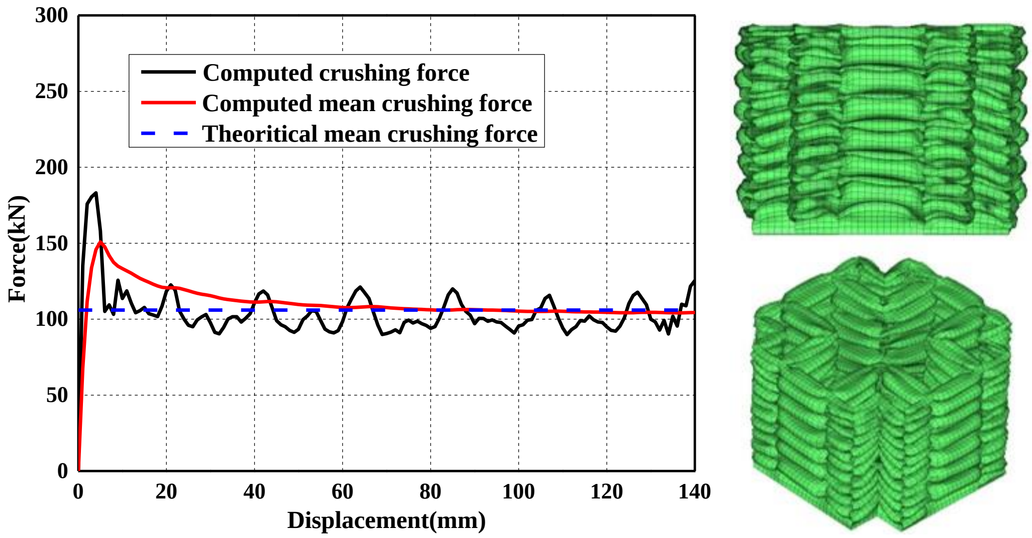

Fig.8 Crushing force and deformed structure with Tube Type Ⅱ

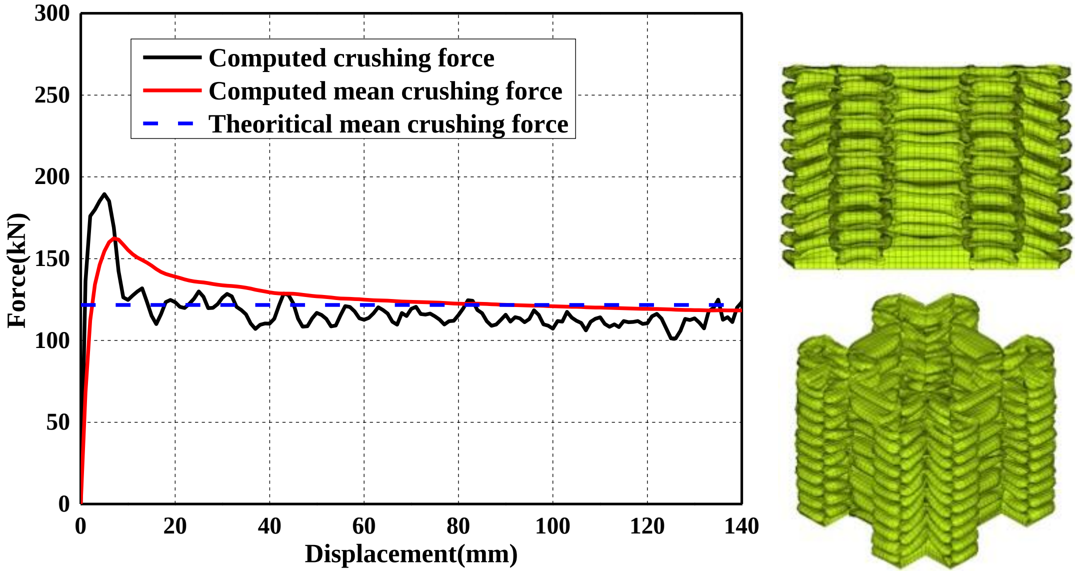

Fig.9 Crushing force and deformed structure with Tube Type Ⅲ

The crushing force-displacement curves of three structures with t=1.6mm are presented in Fig.7-9. From the Fig.7-9, it could be seen that the deformation modes of the multi-cell thin-walled tubes, which were obtained by the numerical simulation, are stable.

According to the analysis above, it can be concluded that the Tube Type Ⅲ is the best energy absorb structure among the three tubes, which is consistent with the theoretical predictions concluded in the previous section. Therefore, further investigation will be carried out for Tube Type Ⅲ in next section.

4. Parametric study and multi-objective optimization of the Type Ⅲ structure

From the above study, it could be seen that the energy absorption capacity of the Tube Type Ⅲ is better than the other two types. To better understand the crashworthiness characteristics of the Tube Type Ⅲ, it is necessary to carried out further study in this section on geometric cross-sectional parameters, including the wall thickness t, the location of the connecting flange wall u and the size of the corner-cell C.

In this section, the basic element numbers of Tube Type Ⅲ keep constant, the wall thickness t, the location of the connecting flange wall u and the size of the corner-cell C were changed to investigate effects of these geometric cross-sectional parameters.

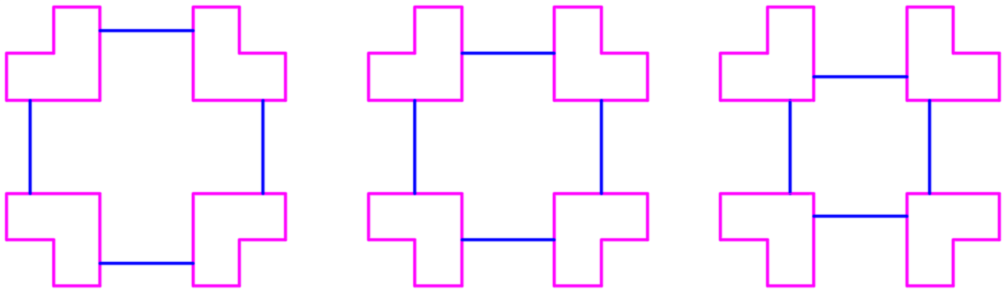

(a) u=0.25 (b) u=0.5 (c) u=0.75

Fig.10 The cross-sections of Tube Type Ⅲ with different locations of the connecting flange walls

In order to generate efficient sample points used for parametric analyses, the full factorial method which is a design of experiments (DOE) is applied. In this paper, six different thicknesses, four corner-cell sizes and three location of the connecting flange wall are considered to investigate their effects. Fig.10 shows the cross-sections of Tube Type Ⅲ with three different locations of the connecting flange walls. Since the crashworthiness indicators are essentially connected with the given deformation distance, the value of deformation distance is set as 120 mm for all the finite element models used for following parametric analyses.

4.1 Effect of the corner-cell size and wall thickness

In order to investigate the crashworthiness of multi-cell thin-walled tubes with four different corner-cell size (C=25 mm, 30 mm, 35 mm, 40 mm), numerical simulations of the tubes with different thickness are performed. Fig.12 (a) and (b) showed the MCF and EA of four different corner-cell sizes of Tube Type Ⅲ with different wall thicknesses. It could be seen that both the values of MCF and EA increase with the increasing o

ll corner-cell sizes. The values of MCF are the largest for the Tube Type Ⅲ with a corner-cell size of 40 mm when the wall thickness is 0.8 mm or more than 1.6 mm, while the multi-cell tubes with the 35 mm corner-cell size is larger than the other tubes when the wall thickness 1.0 mm ≤ t ≤ 1.4 mm. The tendency of EA for different corner-cell size is same as that of MCF, since the values of MCF were calculated by the Eq. (16).

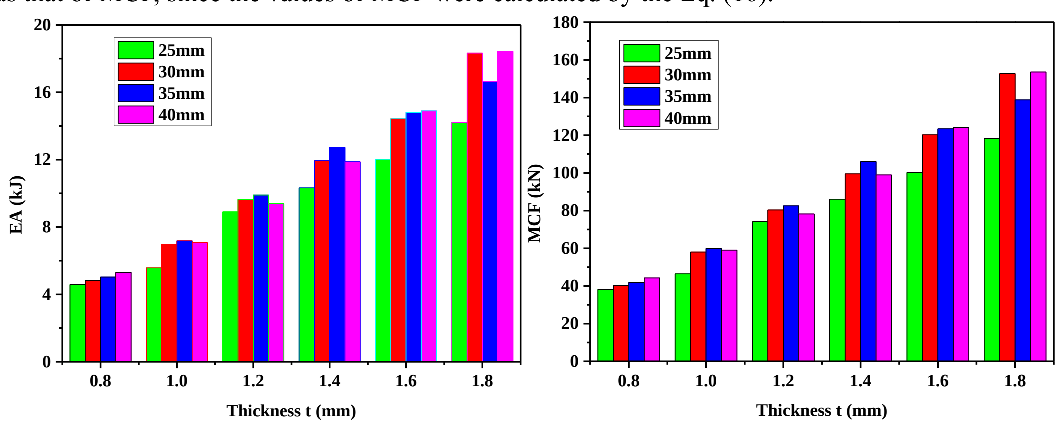

(a) (b)

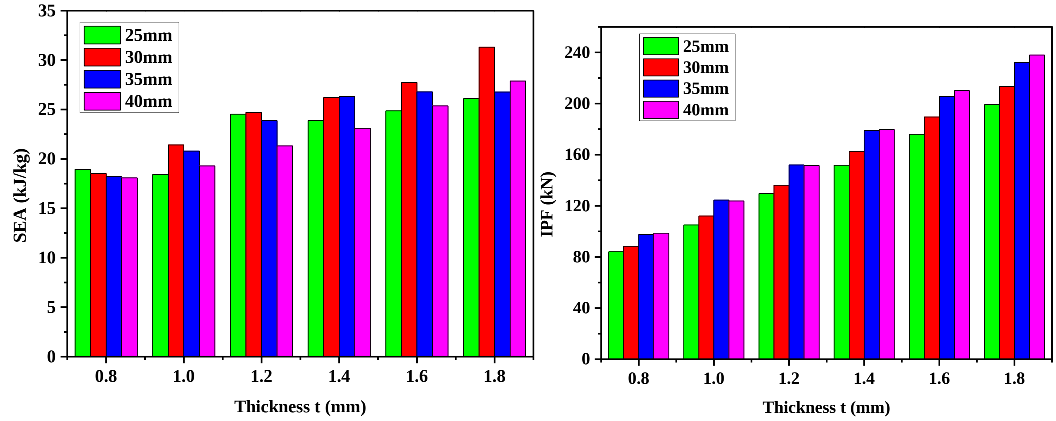

(c) (d)

Fig.11 Comparisons of crashworthiness characteristics of Tube Type Ⅲ with different corner-cell size: (a) MCF; (b) EA; (c) SEA; (d) IPF.

Fig.11 (c) and (d) depict the SEA and IPF of the multi-cell thin-walled tubes with four different corner-cell sizes. According to Fig.11 (c), it can be observed that the multi-cell thin-walled tubes with 30 mm corner-cell size, in general, show the best SEA performance. From the Fig.11 (d), it can be found that the values of IPF increase with the increasing values of wall thickness. And for each of wall thickness, the larger the corner-cell size, the greater the IPF.

4.2 Effect of the location of the connecting flange wall and wall thickness

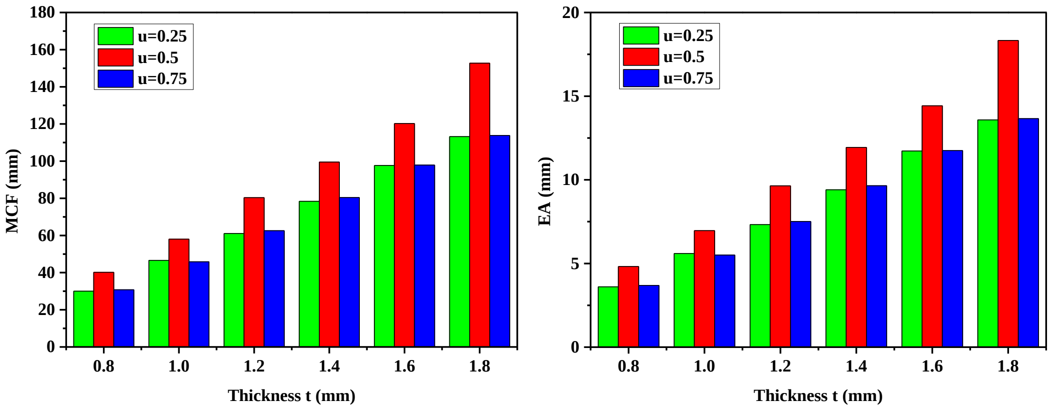

(a) (b)

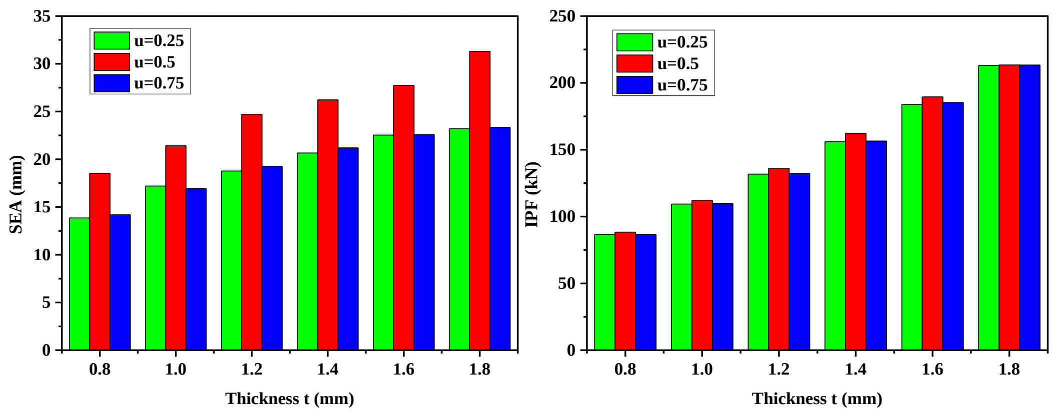

(c) (d)

Fig.12 Comparisons of crashworthiness characteristics of Tube Type Ⅲ with different location of the connecting flange wall: (a) MCF; (b) EA; (c) SEA; (d) IPF.

Fig.12 (a)-(c) give MCF, EA and SEA of multi-cell thin-walled tubes with three different location of the connecting flange wall. It can be found that the values of MCF, EA and SEA of the multi-cell thin-walled tubes with three different location of the connecting flange wall increase with the increasing of the wall thickness. According to the Eq. (14) and Eq. (16), the relation among MCF, EA and SEA can be depicted as:

$$\mathrm{EA} = \mathrm{MCF} \times \mathrm{d} = \mathrm{SEA} \times \mathrm{m} \tag{17}$$

where the axial crushing distance d is set as 120 mm in this study. Moreover, for the same wall thickness and corner-cell size, the weights of the multi-cell thin-walled tubes with different location of the connecting flange wall are constant. Thus, the tendencies of EA, MCF and SEA are exactly the same.

Obviously, for the indicators of MCF, EA and SEA, the multi-cell thin-walled tubes with location of the connecting flange wall u =0.5 show the best performance when the wall thicknesses are constant. Fig.12 (d) depicts the relation between IPF and wall thickness for the multi-cell thin-walled tubes with different location of the connecting flange wall. The trends of IPF for the multi-cell tubes with different location of the connecting flange wall are rising with the increasing wall thickness, while IPF is almost the same for three different location of the connecting flange wall when the wall thicknesses keep constant.

4.3 Effect of the location of the connecting flange wall and corner-cell size

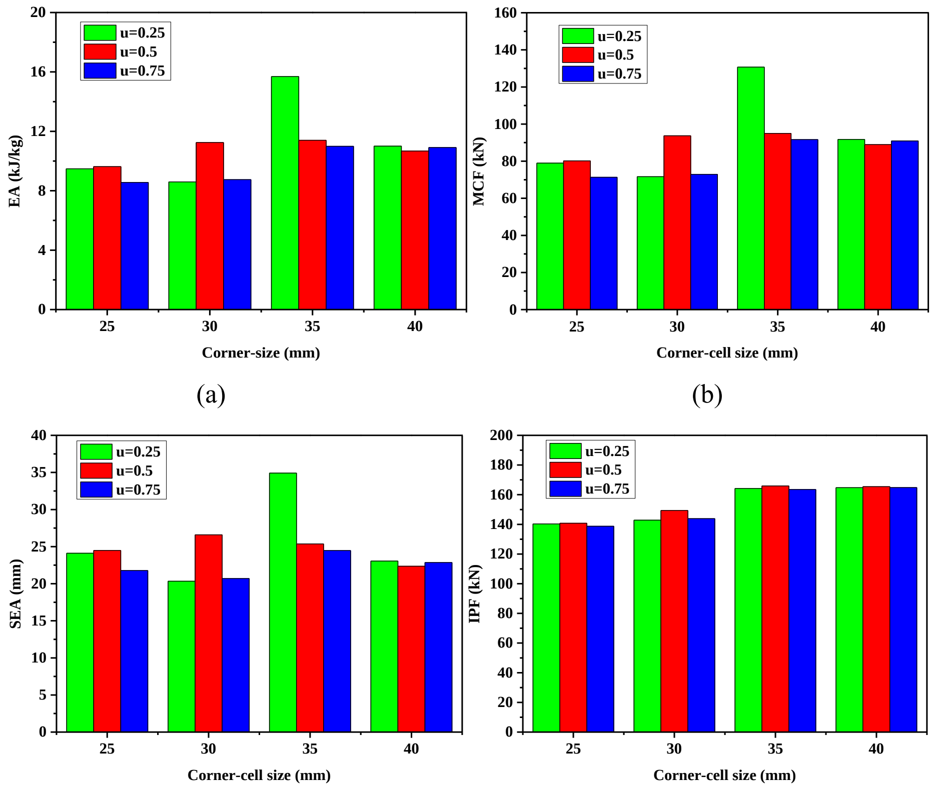

Fig.13 Comparisons of crashworthiness characteristics of Tube Type Ⅲ with different location of the connecting flange wall: (a) MCF; (b) EA; (c) SEA; (d) IPF.

In this section, in order to investigate the effect of the connecting flange and corner-cell size, the wall thickness of all the multi-cell thin-walled tubes are set as 1.3 mm. Since the locations of the connecting flange wall of tubes with same corner-cell size don't change the weights of tubes and the crashing distance is constant, the rules of MCF, EA and SEA are same according to the Eq. (17). From Fig.13 (a)-(c), it can be observed that the multi-cell tubes with $u = 0.25$ and $C = 35$ mm showed the best impacting characteristics. Fig.13 (d) shows IPF of multi-cell thin-walled tubes with three different location of the connecting flange wall for the variation of the corner-cell size. It is concluded that the IPF values of the tubes with different location of the connecting flange wall, for the same corner-cell size, are approximate.

5 Conclusions

In this study, the crashworthiness of three different sectional configurations, multi-cell thin-walled tubes were first investigated by numerical simulation and theoretical analysis methods. In the part of sectional configurations, the folding and translation methods were applied. It is more convenient to compare the crashworthiness of the three multi-cell thin-walled tubes by using this method, since corners of cross-section are just added without changing the weight of tubes. In addition, theoretical expressions of the mean crushing forces of the multi-cell thin-walled tubes were derived by using the Simplified Super Folding Element (SSFE) theory. According to the numerical and theoretical analysis results, it could be concluded that:

The folding and translation methods are efficient for the sectional configurations during the process of multi-cell tubes design.

The Tube Type Ⅲ was the best energy absorber among these three multi-cell tubes.

The wall thickness, the corner-cell size and flange locations have obvious effect on the crashworthiness of the multi-cell thin-walled tubes.

Acknowledgments

The authors would like to thank the financial support from National Science Foundation (No. 51475153) and the S cience Fundation of State Key Laboratory of Advanced Design and Manufacturing for Vehicle Body (No. 71575004).

References

[1] A.G. Mamalis, D.E. Manolakos, M.B. Ioannidis, P.K. Kostazos, and G. Hassiotis, Finite element simulation of the axial collapse of thin-wall square frusta, Int. J. Crashworthiness 6 (2001), pp. 155164.

[2] G.X. Lu, T.X. Yu. Energy absorption of structures and materials. Boca Raton: CRC Press; 2003.

[3] J. Marsolek and H.G. Reimerdes, Energy absorption of metallic cylindrical shells with induced non-axisymmetric folding patterns, Int. J. Impact Eng. 30 (2004), pp. 12091223.

[4] Liu W, Lin Z, He J, et al. Crushing behavior and multi-objective optimization on the crashworthiness of sandwich structure with star-shaped tube in the center[J]. Thin-Walled Structures, 2016, 108: 205-214.

[5] Kim HS. New extruded multi-cell aluminum profile for maximum crash energy absorption and weight efficiency. Thin-walled Struct 2002;40 (4):311–27.

[6] A.G. Hanssen, M. Langseth, O.S. Hopperstad, Static and dynamic crushing of circular aluminum extrusions with aluminum foam filler, Int. J. Impact Eng. 24 (2000) 475–507.

[7] G.L.S.R. Guillow, R.H. Grzebieta, Quasi-static axial compression of thin-walled circular aluminum tubes, Int. J. Mech. Sci. 43 (2001) 2103–2123.

[8] S. Salehghaffari, M. Tajdari, M. Panahi, F. Mokhtarnezhad, Attempts to improve energy absorption characteristics of circular metal tubes subjected to axial loading, Thin-Walled Struct. 48 (2010) 379–390.

[9] L.W. Guo, J.L. Yu, Z.B. Li, Experimental studies on the quasi-static bending behavior of double square tubes filled with aluminum foam, Acta

Mech. 213 (2010) 349–358.
[10] L. Guo, J. Yu, Dynamic bending response of double cylindrical tubes filled with aluminum foam, Int. J. Impact Eng. 38 (2011) 85–94.
[11] M.H. Shojaeefard, A. Najibi, M. Anbarloei, M. Yeganeh, Experimental and numerical crashworthiness investigation of combined circular and square sections, J. Mech. Sci. Technol. 28 (2014) 999–1006.
[12] A. Partovi Meran, T. Toprak, A. Muğan, Numerical and experimental study of crashworthiness parameters of honeycomb structures, Thin-Walled Struct. 78 (2014) 87–94.
[13] .P. Santosa, Experimental and numerical studies of foam-filled sections, Int. J. Impact Eng. 24 (2000) 509–534.
[14] X. Zhang, H. Zhang, Numerical investigations on a new type of energy-absorbing structure based on free inversion of tubes, Int. J. Mech. Sci. 51 (2009) 64–76.
[15] Z. Tang, S. Liu, Z. Zhang, Energy absorption properties of non-convex multi-corner thin-walled columns, Thin-Walled Struct. 51 (2012) 112–120.
[16] A. Partovi Meran, T. Toprak, A. Muğan, Numerical and experimental study of crashworthiness parameters of honeycomb structures, Thin-Walled Struct. 78 (2014) 87–94.
[17] X. Zhang, H. Zhang, Z. Wen, Experimental and numerical studies on the crush resistance of aluminum honeycombs with various cell configurations, Int. J. Impact Eng. 66 (2014) 48–59.
[18] N. Rathinam, B. Prabu, Numerical study on influence of dent parameters on critical buckling pressure of thin cylindrical shell subjected to uniform lateral pressure, Thin-Walled Struct. 88 (2015) 1–15.
[19] H. Zhao, S. Abdennadher, On the strength enhancement under impact loading of square tubes made from rate insensitive metals, Int. J. Solids Struct. 41 (2004) 6677–6697.
[20] X. Zhang, G. Cheng, H. Zhang, Theoretical prediction and numerical simulation of multi-cell square thin-walled structures, Thin-Walled Struct. 44 (2006) 1185–1191.
[21] H. Yin, G. Wen, Theoretical prediction and numerical simulation of honey-comb structures with various cell specifications under axial loading, Int. J. Mech. Mater. Des. 7 (2011) 253–263.
[22] X. Zhang, H. Zhang, Energy absorption limit of plates in thin-walled structures under compression, Int. J. Impact Eng. 57 (2013) 87–98.
[23] T. Tran, S. Hou, X. Han, W. Tan, N. Nguyen, Theoretical prediction and crash-worthiness optimization of multi-cell triangular tubes, Thin-Walled Struct. 82 (2014) 183–195.
[24] J.M. Alexander. An approximate analysis of the collapse of thin cylindrical shells under axial loading. Quarterly Journal of Mechanics and Applied Mathematics 1960, 13(1): 10-15.
[25] T. Wierzbicki, W. Abramowicz. On the crushing mechanics of thin-walled structures. Journal of Applied Mechanics 1983, 50(4a): 727-734.
[26] W. Chen, T. Wierzbicki. Relative merits of single-cell, multi-cell and foam-filled thin-walled structures in energy absorption. Thin-Walled Structures 2001; 39(4): 287-306.
[27] Zhang X, Cheng G, Zhang H. Theoretical prediction and numerical simulation of multi-cell square thin-walled structures[J]. Thin-Walled Structures, 2006, 44(11): 1185-1191.
[28] X. Zhang, G. Cheng, A comparative study of energy absorption characteristics of foam-filled and multi-cell square columns, Int. J. Impact Eng. 34 (2007) 1739–1752.
[29] Zhang X, Zhang H. Energy absorption of multi-cell stub columns under axial compression. Thin Wall Structures, 2013;68:156–63.
[30] Wu S, Zheng G, Sun G, et al. On design of multi-cell thin-wall structures for crashworthiness[J]. International Journal of Impact Engineering, 2016, 88: 102-117.
[31] K. Yamazaki, J. Han, Maximization of the crushing energy absorption of tubes, Struct. Optim. 16 (1) (1998) 37–46
[32] P. Marklund, L. Nilsson, Optimization of a car body component subjected to side impact, Struct. Multidiscip. Optim. 21 (5) (2001) 383–392.
[33] Zarei HR, Kroger M, Optimization of the foam-filled aluminum tubes for crush box application. Thin Wall Struct 46(2):214–221
[34] Zhang Y, Sun GY, Xu XP, Li GY, Li Q, Multiobjective crashworthiness optimization of hollow and conical tubes for multiple load cases. Thin-Walled Struct 82:331–342

[35] J. Fang, Y. Gao, G. Sun, N. Qiu, Q. Li, On design of multi-cell tubes under axial and oblique impact loads, Thin-Walled Structures 95 (2015) 115–126.

[36] Chen Y, Clausen AH, Hopperstad OS, Langseth M. Stress–strain behavior of aluminum alloys at a wide range of strain rates. Int J Solids Struct 2009;46:3825–35

[37] A.G. Hanssen, M. Langseth, O.S. Hopperstad, Static and dynamic crushing of circular aluminum extrusions with aluminum foam filler, International Journal of Impact Engineering 24 (2000) 475–507.

[38] I. McGregor, IMPACT PERFORMANCE OF ALUMIIMIUM STRUCTURES, in: Structural Crashworthiness and Failure: Proceedings of the Third International Symposium on Structural Crashworthiness held at the University of Liverpool 14-16 April 1993, CRC Press, England (2010), p. 333.

[39] T. Tran, S. Hou, X. Han, M. Chau, Crushing analysis and numerical optimization of angle element structures under axial impact loading, Composite Structures 119 (2015) 422–435.

[40] Albert, Prescilla Christy, et al. "Axial Crushing Behavior of Aluminum Square Tube with Origami Pattern." Modern Applied Science 10.2 (2016): 90.

[41] Duan, Libin, et al. "Design optimization of tailor-rolled blank thin-walled structures based on-support vector regression technique and genetic algorithm." Engineering Optimization (2016): 1-18.

[42] Pang, Tong, et al. "Crashworthiness design of functionally graded structures with variable diameters." International Journal of Crashworthiness (2016): 1-15.

[43] Abramowicz W, Wierzbicki T. Axial crushing of multi-corner sheet metal columns[J]. Journal of Applied Mechanics, 1989, 56(1): 113-120.

[44] Qiu N, Gao Y, Fang J, et al. Theoretical prediction and optimization of multi-cell hexagonal tubes under axial crashing[J]. Thin-Walled Structures, 2016, 102: 111-121.

[45] Tran T N, Hou S, Han X, et al. Theoretical prediction and crashworthiness optimization of multi-cell square tubes under oblique impact loading[J]. International Journal of Mechanical Sciences, 2014, 89: 177-193.

[46] Yin H, Wen G, Liu Z, et al. Crashworthiness optimization design for foam-filled multi-cell thin-walled structures[J]. Thin-Walled Structures, 2014, 75: 8-17.

[47] Ali M, Ohioma E, Kraft F, et al. Theoretical, numerical, and experimental study of dynamic axial crushing of thin walled pentagon and cross-shape tubes[J]. Thin-Walled Structures, 2015, 94: 253-272.